Supporting information for the paper:

Water-assisted proton conduction regulated by hydrophilic groups in metallo-hydrogen-bonded organic frameworks: "Like-attracts-like" between hydrophilic group and water molecule

Sen Wang, [a] Fengxia Xie, [*a] Shiwen Zhang, [a] Xiaoqiang Liang, [*a] Qianhang Gao, [a] Yu Chen, [a] Feng Zhang, [c] Chen Wen, [*b] Lei Feng [b] and Chengan Wan [b]

[a] *College of Environmental and Chemical Engineering, Xi'an Polytechnic University, Xi'an 710048, PR China. E-mail: anxiny@163.com, xq-liang@163.com*
[b] *Beijing Spacecrafts, Beijing 100094, PR China. E-mail: 13552907280@163.com*
[c] *Key Laboratory of Photochemical Biomaterials and Energy Storage Materials, Heilongjiang Province and College of Chemistry and Chemical Engineering, Harbin Normal University, Harbin 150025, PR China*

Table of Contents

I. Crystallographic data

Table S1 Selected bond lengths (Å) and angles (°) for **Co-2PPA** and **Co-4PPA**.

		Co-2PPA	
Co(1)−O(1)	2.115(3)	Co(1)−N(1)	2.094(3)
Co(1)−N(2)	2.208(3)	Co(1)−O(1a)	2.115(3)
Co(1)−N(1a)	2.094(3)	Co(1)−N(2a)	2.208(3)
O(1)−Co(1)−N(1)	87.45(10)	O(1)−Co(1)−N(2)	90.35(7)
O(1)−Co(1)−O(1a)	180.00	O(1)−Co(1)−N(1a)	92.55(10)
O(1)−Co(1)−N(2a)	89.65(7)	N(1)−Co(1)−N(2)	89.65(7)
O(1a)−Co(1)−N(1)	92.55(10)	N(1)−Co(1)−N(1a)	180.00
N(1)−Co(1)−N(2a)	90.35(7)	O(1a)−Co(1)−N(2)	89.65(7)
N(1a)−Co(1)−N(2)	90.35(7)	N(2)−Co(1)−N(2a)	180.00
O(1a)−Co(1)−N(1a)	87.45(10)	O(1a)−Co(1)−N(2a)	90.35(7)
N(1a)−Co(1)−N(2a)	89.65(7)	Co(1)−N(1)−C(1)	162.33(18)
Co(1)−O(1)−H(1B)	124.00	Co(1)−O(1)−H(1A)	125.00
Co(1)−N(2)−C(2)	124.51(14)	Co(1)−N(2)−C(3)	118.46(14)
		Co-4PPA	
Co(1)−N(1)	2.094(14)	Co(1)−N(6)	2.1979(12)
Co(1)−N(2)	2.2479(13)	Co(1)−N(1a)	2.0940(14)
Co(1)−N(2a)	2.2479(13)	Co(1)−N(6a)	2.1979(12)
N(1)−Co(1)− N(2)	91.33(5)	N(1)−Co(1)− N(6)	88.57(5)
N(1)−Co(1)− N(1a)	180.00	N(1)−Co(1)− N(2a)	88.67(5)
N(1)−Co(1)− N(6a)	91.44(5)	N(2)−Co(1)− N(6)	86.54(4)
N(1a)−Co(1)− N(2)	88.67(5)	N(2)−Co(1)− N(2a)	180.00
N(2)−Co(1)− N(6a)	93.46(4)	N(1a)−Co(1)− N(6)	91.44(5)
N(2a)−Co(1)− N(6)	93.46(4)	N(6)−Co(1)− N(6a)	180.00
N(1a)−Co(1)− N(2a)	91.33(5)	N(1a)−Co(1)− N(6a)	88.57(5)
N(2a)−Co(1)− N(6a)	86.54(4)	Co(1)−N(1)− C(1)	143.81(12)
Co(1)−N(1)− C(2)	120.82(10)	Co(1)−N(1)− C(3)	120.82(10)
Co(1)−N(6)− C(11)	123.28(9)	Co(1)−N(1)− C(12)	118.71(9)

Symmetry codes : a) 2–*x*,–*y*,1–*z* for **Co-2PPA**; a) 1–*x*,1–*y*,1–*z* for **Co-4PPA.**

Table S2 Hydrogen-bonding geometry parameters (Å, °) for **Co-2PPA** and **Co-4PPA**.

D−H···A	d(D−H)	d(H···A)	d(D···A)	∠(DHA)
		Co-2PPA		
O(1)−H(1B)···O(2a)	0.81	1.92	2.723(4)	175
O(2)−H(2B)···N(3b)	0.97	2.02	2.960(4)	164
N(5)−H(5B)···N(4c)	0.78	2.36	3.139(4)	179
		Co-4PPA		
N(5)−H(5B)···N(8a)	0.86	2.37	3.222(2)	169
N(9)−H(9A)···N(4b)	0.82	2.13	2.944(2)	171
N(9)−H(9B)···N(7c)	0.81	2.32	3.118(2)	166

Symmetry codes: a) 1+*x*, *y*, *z*; b) –1+*x*, *y*, *z*; c) 1–*x*, 1–*y*, –*z* for **Co-2PPA**; a) 2+*x*, *y*, –1+*z* ; b) –2+*x*, *y*, 1+*z* ; c) –*x*, 1–*y*, 2–*z* for **Co-4PPA**.

Crystal Structures

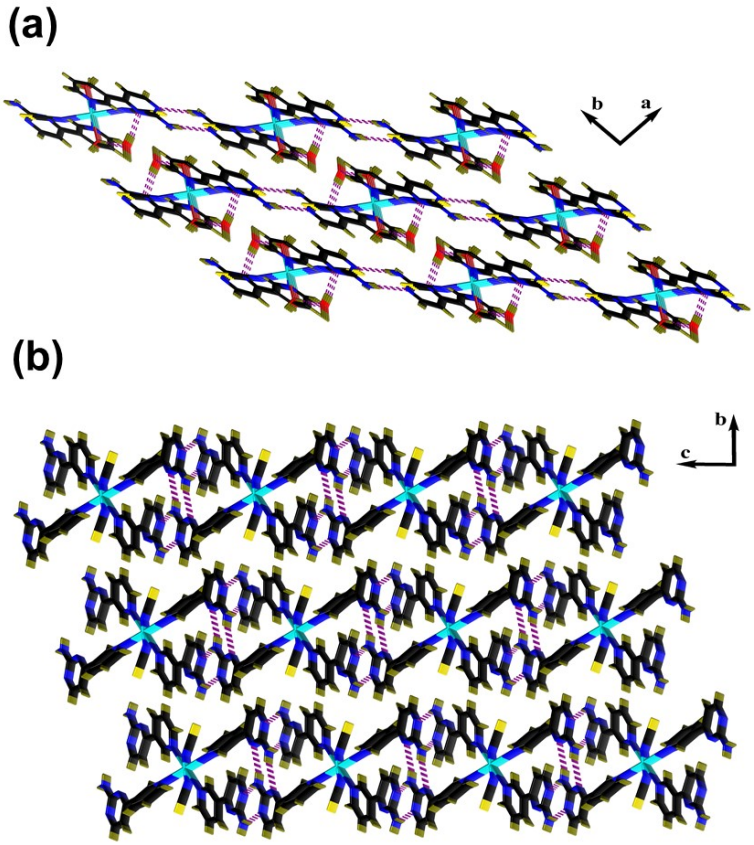

Fig. S1 The 3D hydrogen-bonding framework formed by O−H···O and O−H···N hydrogen-bonding interactions in **Co-2PPA** (a) and the 3D hydrogen-bonding framework via N−H···N hydrogen bonds in **Co-4PPA** (b).

II. Characterization: PXRD patterns

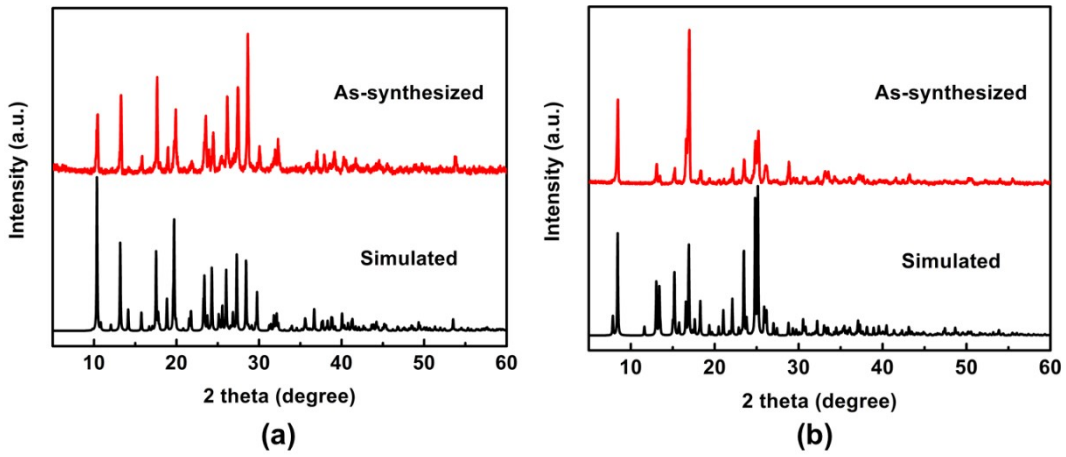

Fig. S2 The PXRD patterns for **Co-2PPA** (a) and **Co-4PPA** (b) of a simulation based on single-crystal analysis and as-synthesized bulk crystals.

III. Characterization: IR Spectra

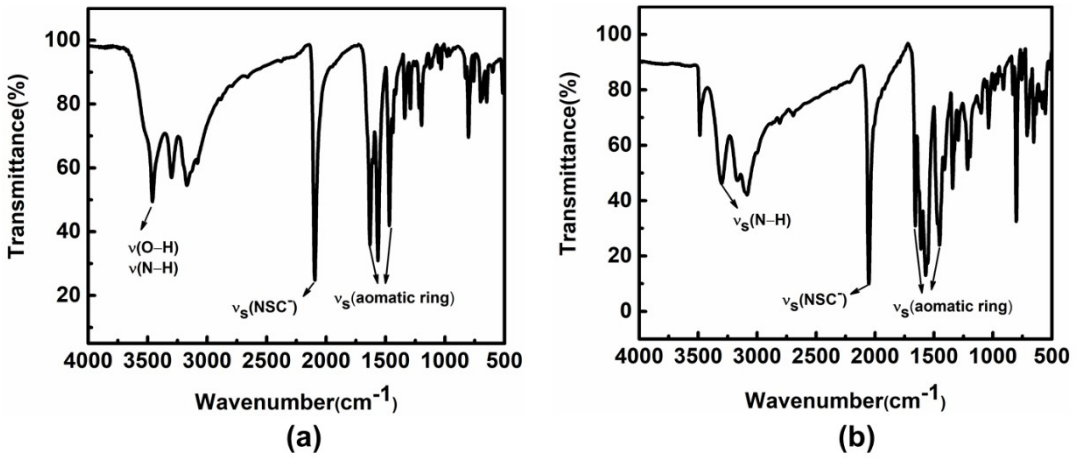

Fig. S3 IR absorption spectrum of **Co-2PPA** (a) and **Co-4PPA** (b) in the solid state at room temperature.

IV. Characterization: SEM images

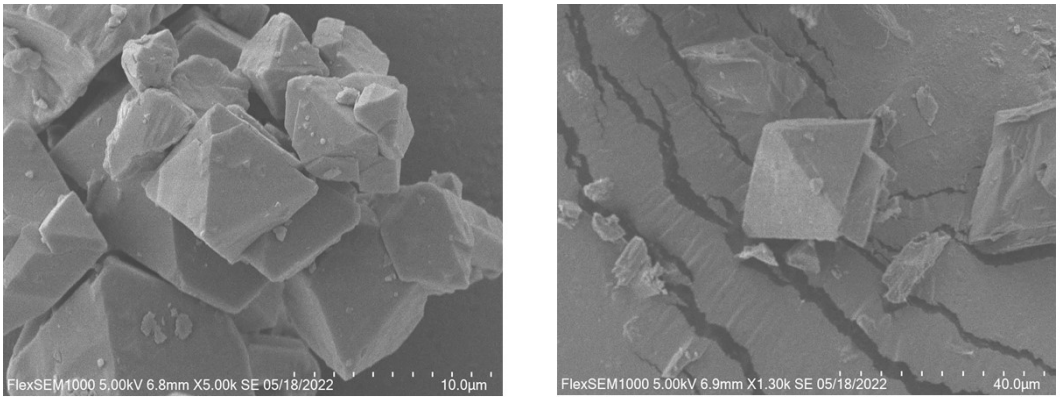

Fig. S4 SEM photomicrographs of **Co-2PPA** (a) and **Co-4PPA** (b) surface morphology.

V. Characterization: Nitrogen sorption measurements

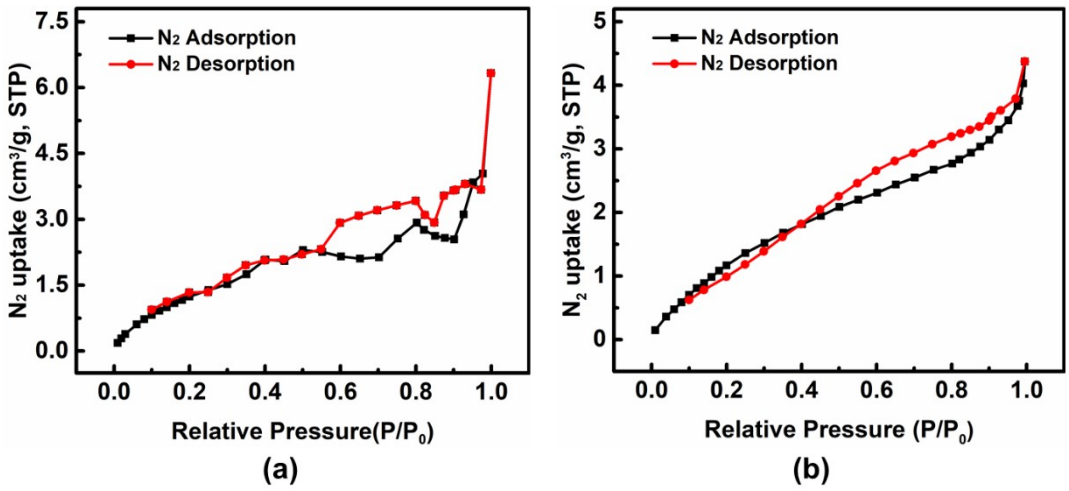

Fig. S5 Nitrogen physisorption isotherms for **Co-2PPA** (a) and **Co-4PPA** (b).

The porosity of Co-2PPA and Co-4PPA was examined by nitrogen sorption experiments at 77 K. As shown in Fig. 5S, the pseudo type-III gas adsorption behaviors for Co-2PPA and Co-4PPA are indicative of their non-porous characteristics. Additionally, the very small BET surface areas were observed in Co-2PPA and Co-4PPA, which are 9.2276 and 7.7428 m^2 /g, respectively, (Langmuir surface areas of 20.2223 and 26.5784 m^2 /g, respectively) (Table S3). This suggests that their adsorption properties are possibly related to the surface of bulk materials rather than the porosity.

Table S3 BET and Langmuir surface areas of Co-2PPA and Co-4PPA

Sample	Type of surface area	Surface area
Co-2PPA	BET (m^2 /g)	9.2276
	Langmuir (m^2 /g)	20.2223
Co-4PPA	BET (m^2 /g)	7.7428
	Langmuir (m^2 /g)	26.5784

VI. Stability: PXRD pattern of Co-2PPA and Co-4PPA after being soaked in different organic solvents

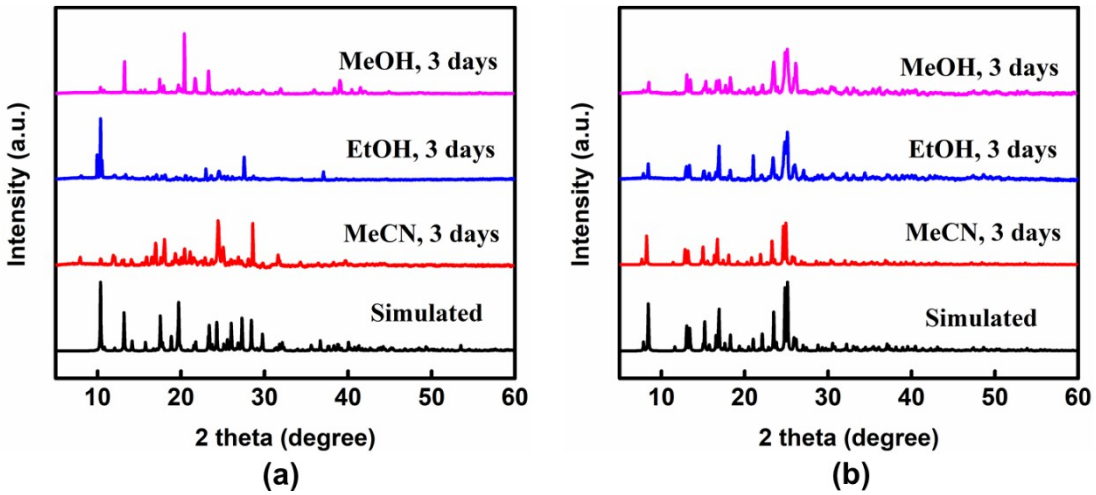

Fig. S6 PXRD patterns of **Co-2PPA** (a) and **Co-4PPA** (b) treated with various organic solvent.

Co-2PPA and Co-4PPA were also suspended in the common organic solvents, such as ethanol, methanol, acetonitrile to monitor their structural integrities. The unchanged PXRD patterns indicate that Co-4PPA can retain its structure after treatment with the common organic solvents. This is because PPA ligands coordinating to Co center have a lower solubility of in organic solvents, such as ethanol, methanol, acetonitrile compared with coordinated water molecules, which leads to the inertness of the PPA ligand and difficulty in reaction with organic solvents to form new compounds. In contrast, water molecule is very soluble in organic solvents and exchange with them to generate new compound. Thus, some peaks similar to the original one and some unidentified peaks are found in the PXRD patterns of the treated Co-2PPA sample. It should be pointed out that Co-2PPA partially maintains its stability and partially undergoes structural phase transitions to produce new crystal structures rather other structural collapse.

VII. Electrochemical measurements: impedance spectra

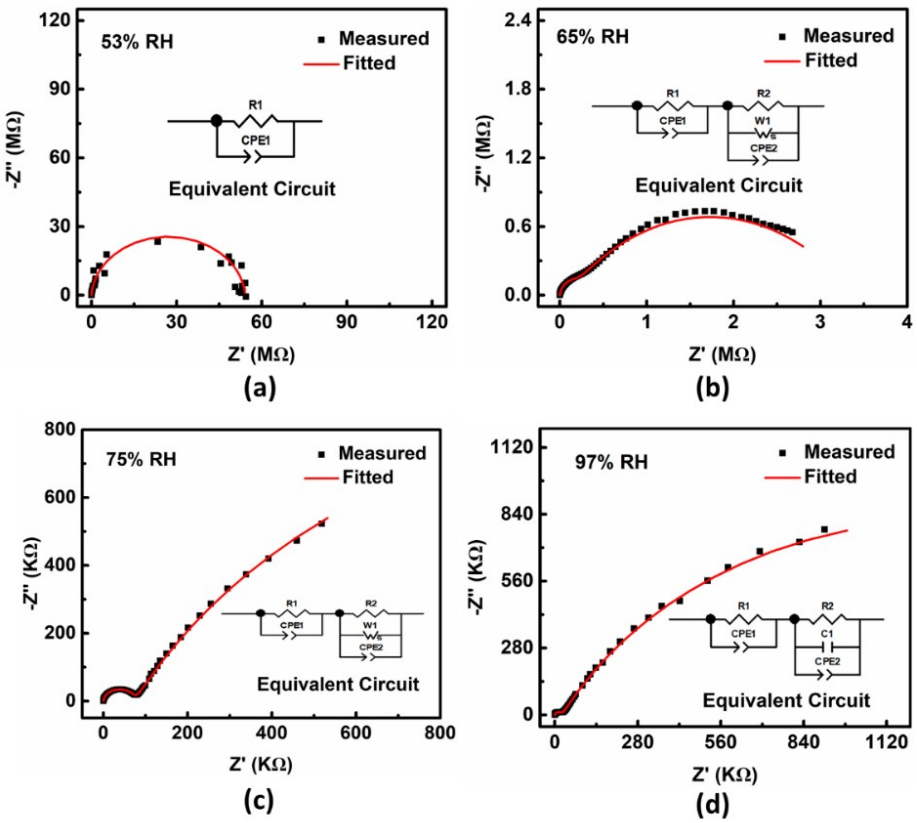

Fig. S7 Nyquist plots of **Co-2PPA** at different RH (relative humidity) and 298 K (R1, bulk resistor; R2, grain boundary resistor; CPE, constant phase element; C1, capacitor; W1, Warburg diffusion element).

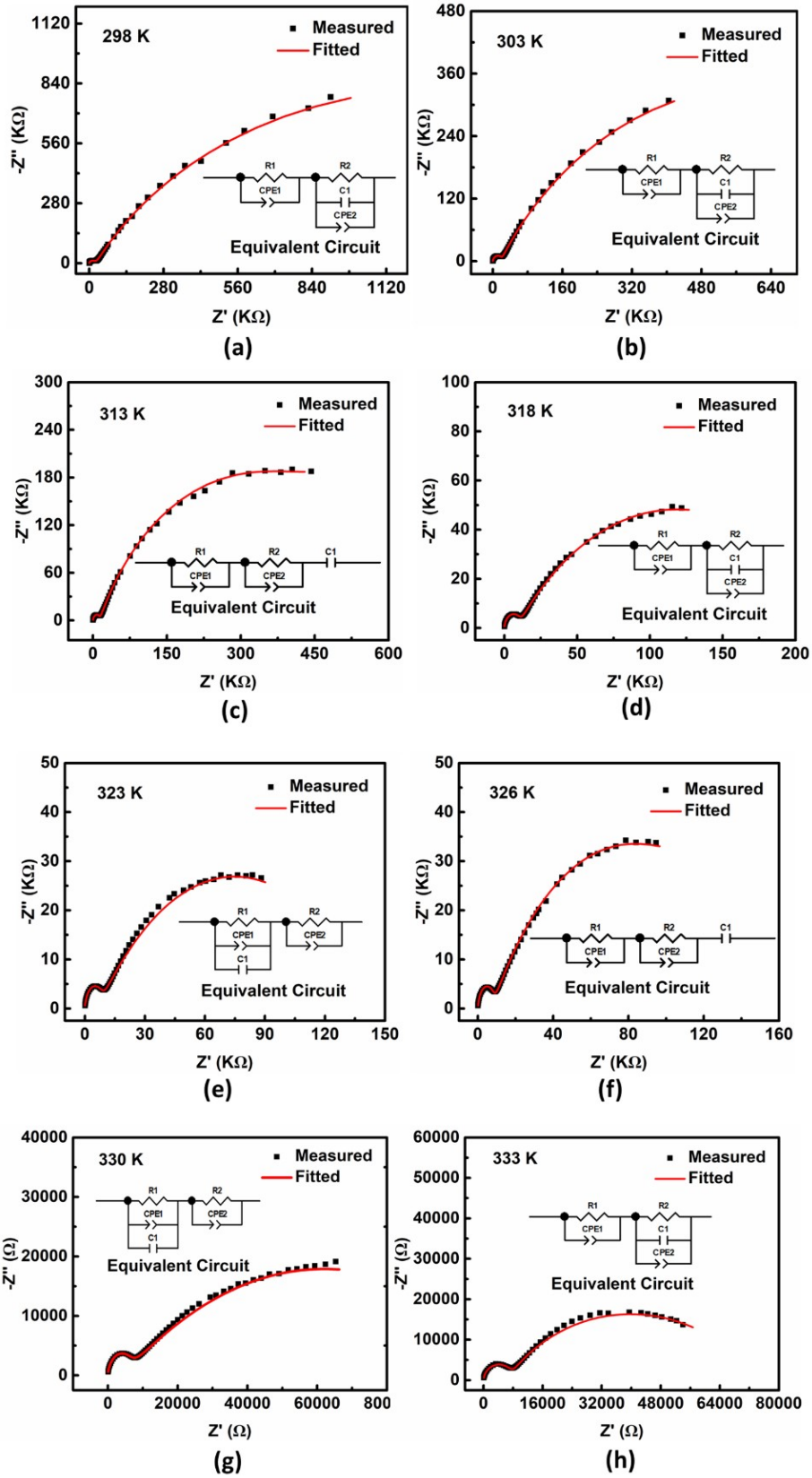

Fig. S8 Nyquist plots of **Co-2PPA** at different temperatures and ~97% RH (relative humidity) (R1, bulk resistor; R2, grain boundary resistor; CPE, constant phase element; C1, capacitor).

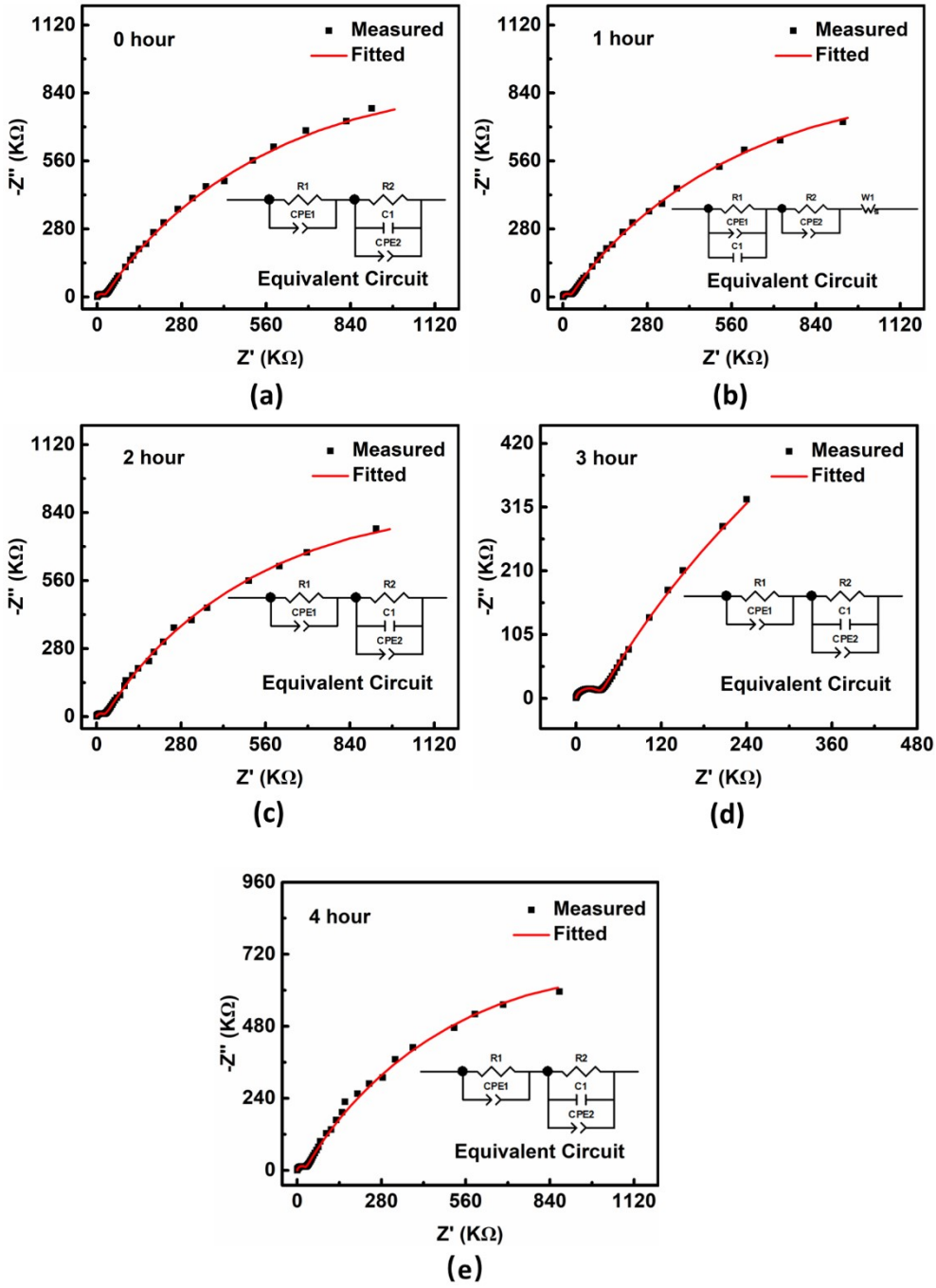

Fig. S9 Nyquist plots of **Co-2PPA** at different time (0-4 hours) and at 298 K~97% RH (relative humidity) (R1, bulk resistor; R2, grain boundary resistor; CPE, constant phase element; C1, capacitor; W1, Warburg diffusion element).

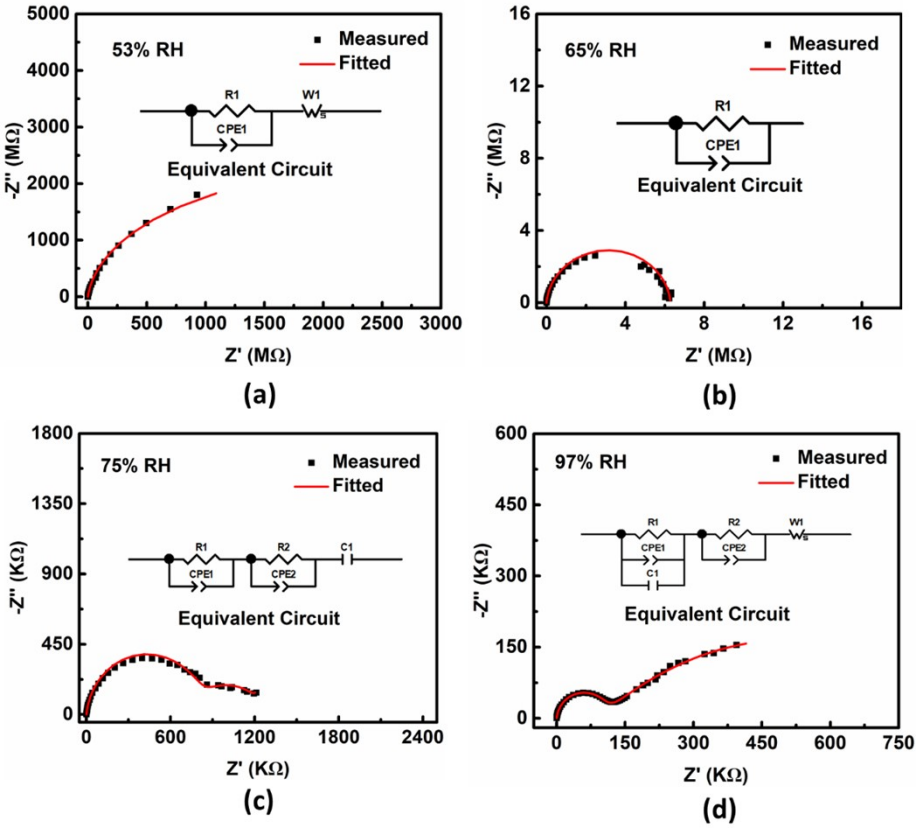

Fig. S10 Nyquist plots of **Co-4PPA** at different RH (relative humidity) and 298 K (R1, bulk resistor; R2, grain boundary resistor; CPE, constant phase element; C1, capacitor; W1, Warburg diffusion element).

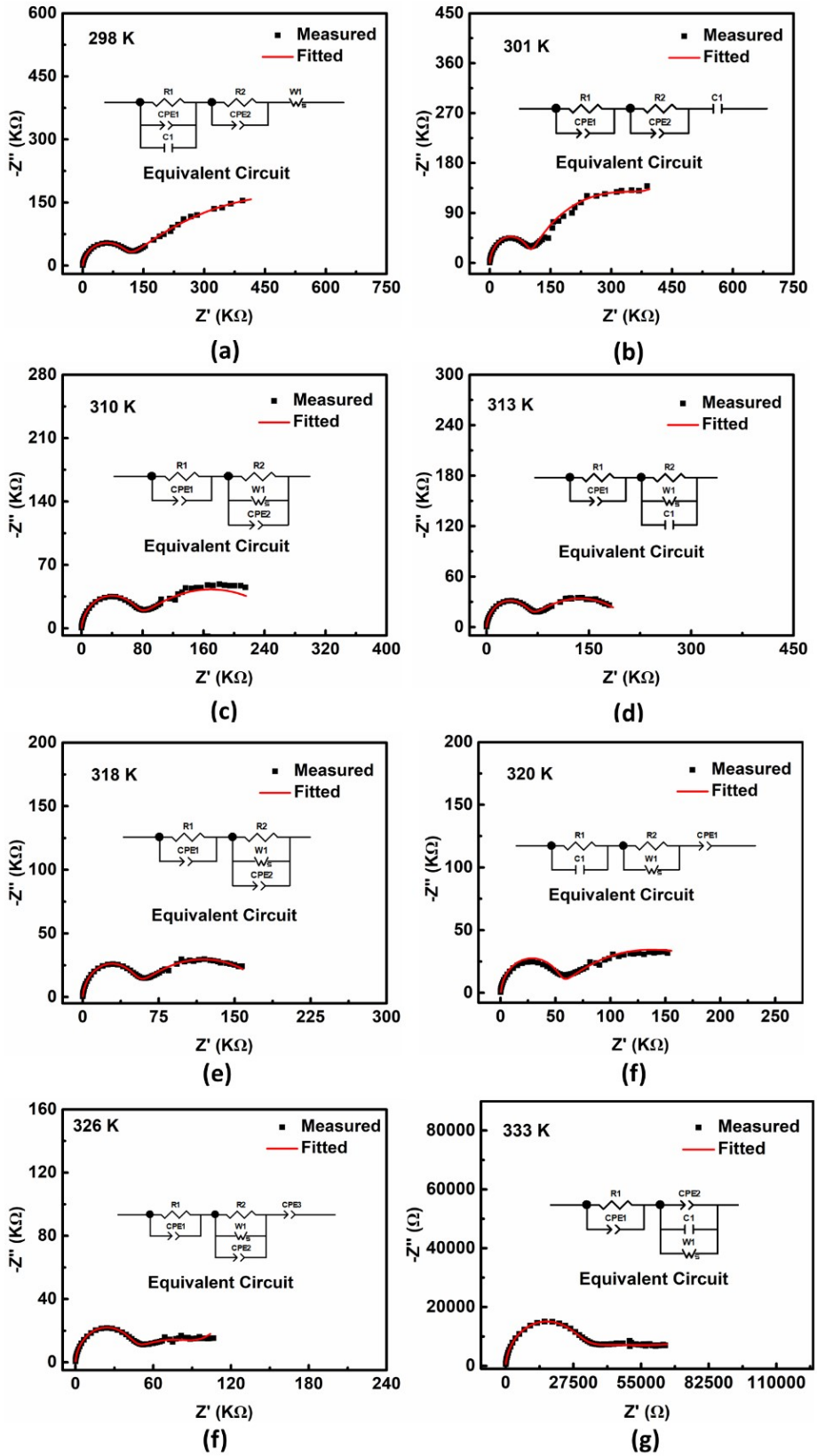

Fig. S11 Nyquist plots of **Co-4PPA** at different temperatures and ~97% RH (relative humidity) (R1, bulk resistor; R2, grain boundary resistor; CPE, constant phase element; C1, capacitor; W1, Warburg diffusion element).

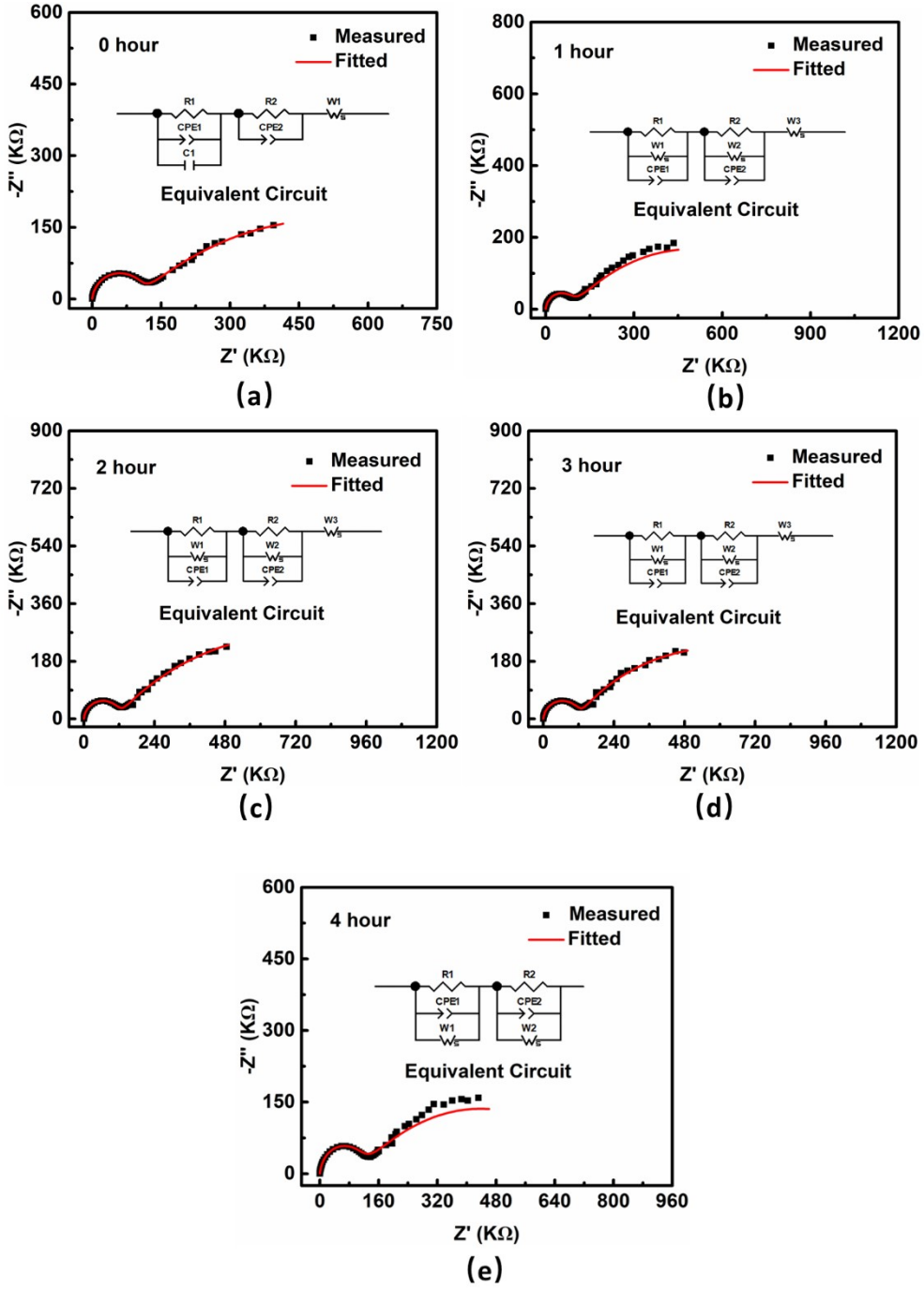

Fig. S12 Nyquist plots of **Co-4PPA** at different time and at 298 K and ~97% RH (relative humidity) (R1, bulk resistor; R2, grain boundary resistor; CPE, constant phase element; C1, capacitor; W1, Warburg diffusion element).

VIII. PXRD patterns after impedance measurements.

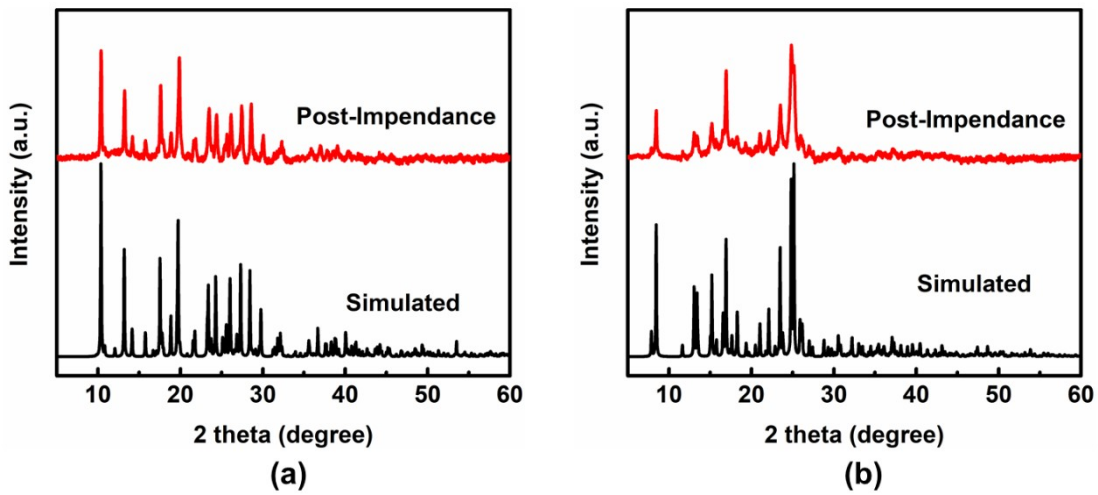

Fig. S13 PXRD patterns of simulations based on single-crystal analysis and after the impedance measurements for **Co-2PPA** (a) and **Co-4PPA** (b) (at ~97% RH and 298–323 K for 0–4 hours).

IX. Water adsorption–desorption isotherms

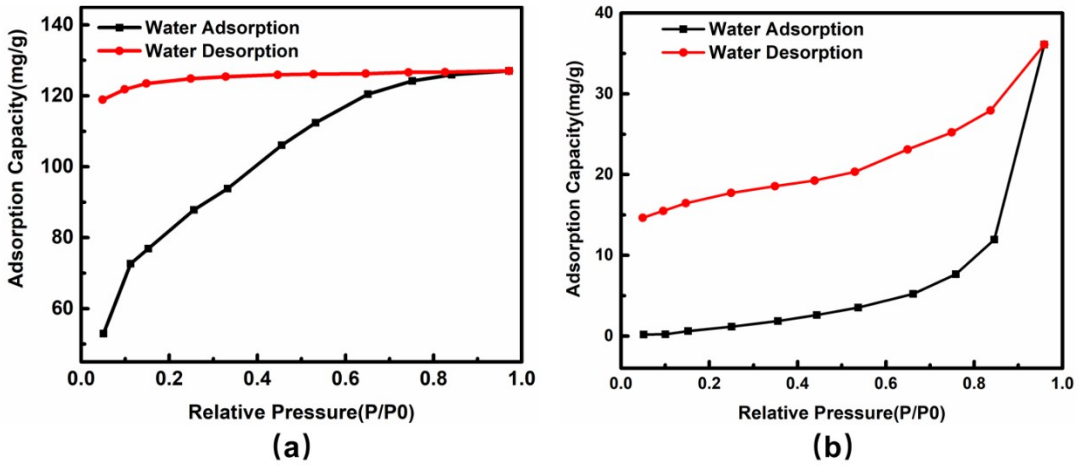

Fig. S14 Water adsorption–desorption isotherms of **Co-2PPA** (a) and **Co-4PPA** (b) at 298 K.

X. Differential Scanning Calorimeter measurements

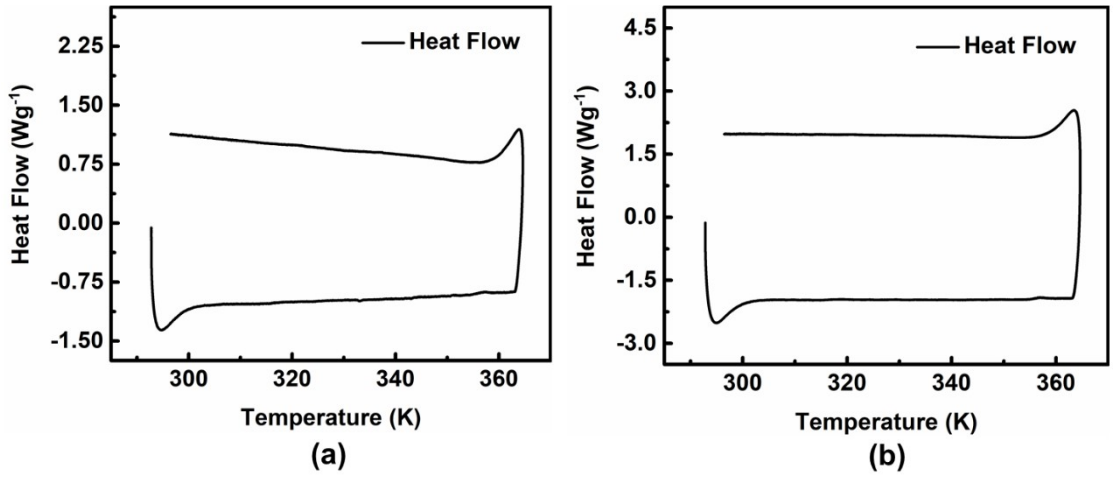

Fig. S15 DSC (Differential Scanning Calorimeter) curves of **Co-2PPA** (a) and **Co-4PPA** (b).

In order to identify the reversible phase transition, we performed differential scanning calorimetry (DSC) measurements on Co-2PPA and Co-4PPA from 293 K to 368 K. It should be pointed out that both Co-2PPA and Co-4PPA contain tiny peaks at 285 K and 368 K, respectively, which are caused on by unstable airflow during the initial heating and final cooling procedure of the instrument. Additionally, no obvious peaks for Co-2PPA and Co-4PPA were detected in DSC curves (Fig. S15), implying that there is the absence of the reversible phase transition.

XI. Dielectric Properties

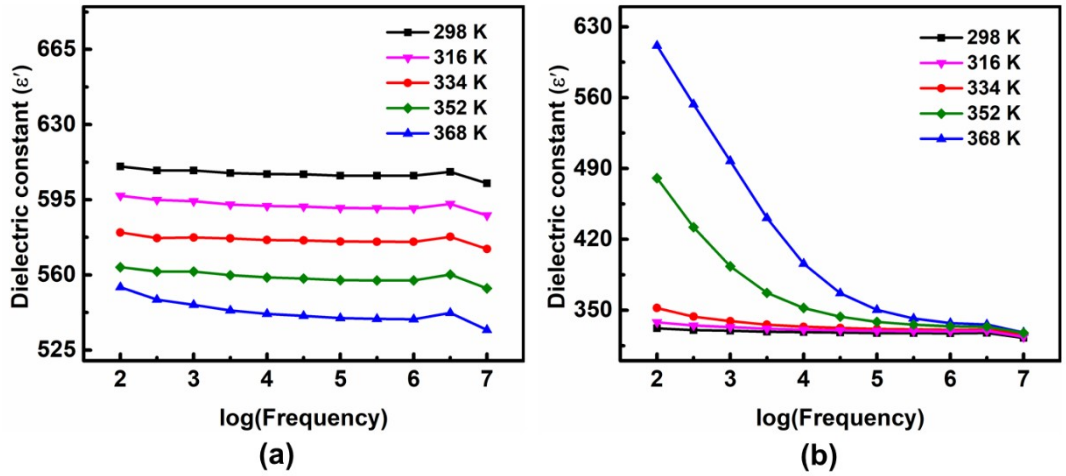

Fig. S16 Frequency dependence of the real part of the dielectric constants (ε′) for (a) Co-2PPA and (b) Co-4PPA at different temperatures.

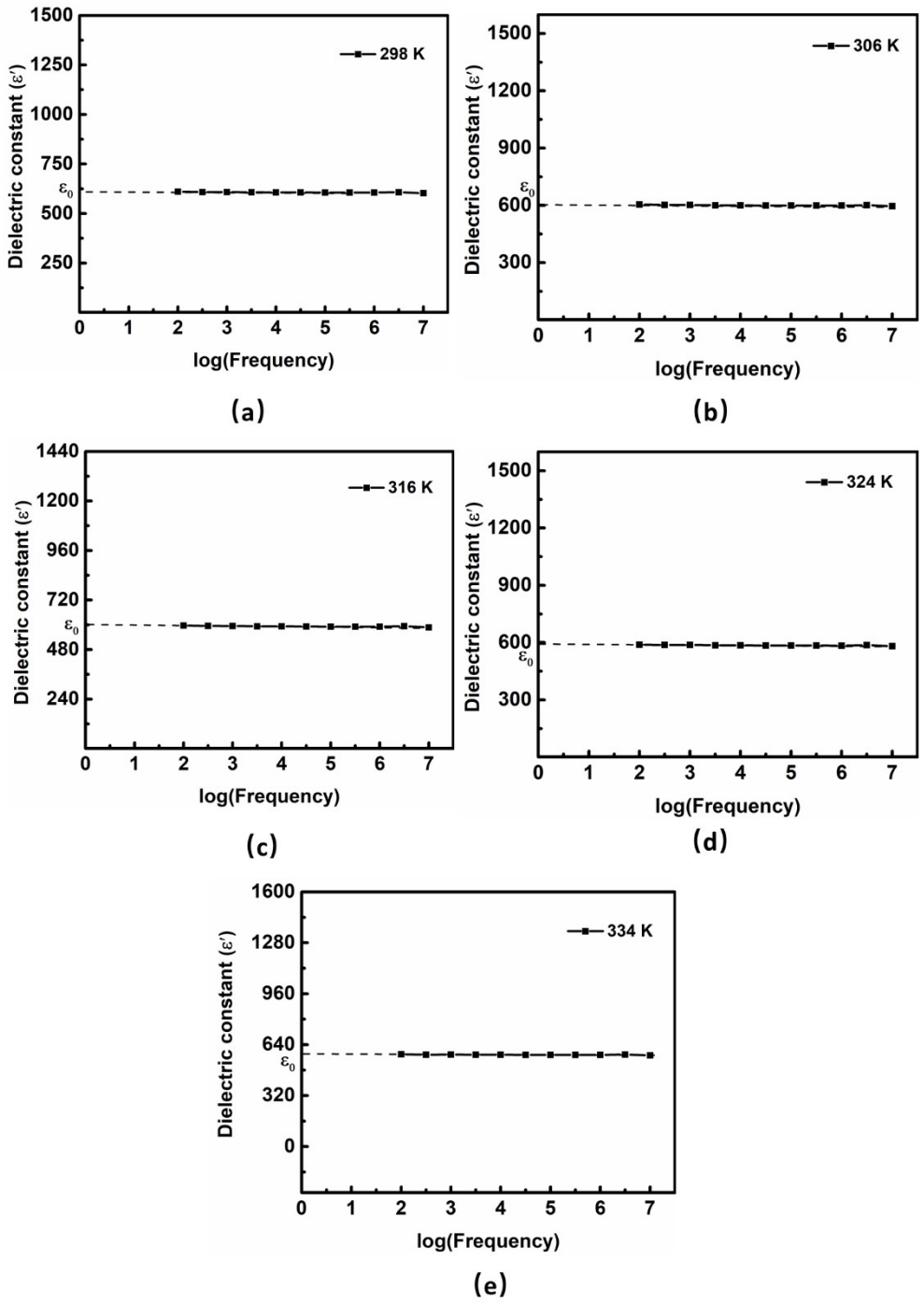

Fig. S17 Frequency dependence of the real part of the static dielectric constants (ε_0) for Co-2PPA and at different temperatures (298-334K).

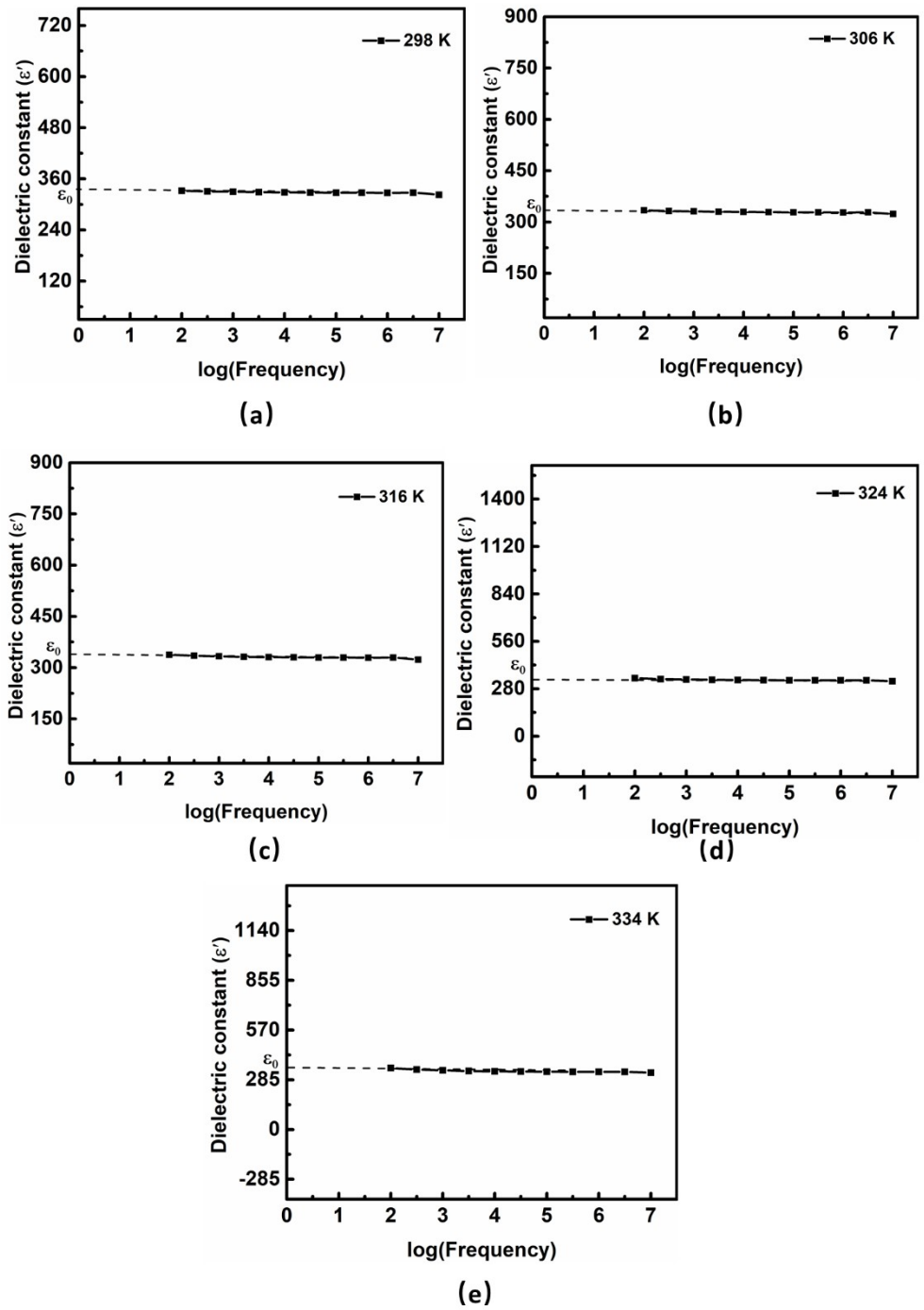

Fig. S18 Frequency dependence of the real part of the static dielectric constants (ε_0) for Co-4PPA and at different temperatures (298-334K).

XII. Comparison of chemical stability

Table S4 Comparison of chemical stability of Co-2PPA and Co-4PPA with reported MOF materials

Materials	pH range	Time (day or hour)	References
Co-2PPA	3-11	12 hours	This work
Co-4PPA	3-11	12 hours	This work
PCN-333(Al)	3-9	overnight	[1]
PCN-777	3-11	12 hours	[2]
$[(CH_3)_2NH_2]_2[Eu_6(m_3\text{-}OH)_8(NDC)_6(H_2O)_6]$ [a]	3.5-10 (373K)	24 hours	[3]
Al-TCPP [b]	5-8 (RT)	1 week	[4]
oCB-MOF-1 [c]	2-12 (RT)	15 hours	[5]
JLU-MOF50 [d]	0-11	48 hours	[6]
FJU-66	3-14	12 hours	[7]
467-MOF [e]	1-11	36 hours	[8]
BUT-155	4-10	24 hours	[9]
BUT-110(Zr)	1-10	48 hours	[10]

[a] 1,4-NDC = 1,4-naphthalenedicarboxylate. [b] H_2TCPP = meso-tetra(4-carboxyl-phenyl)porphyrin. [c] oCB-L = 2-bis{(pyridin-3-yl)methanol}-1,2-dicarba-closo-dodecarborane, H_2ip = isophthalic acid. [d] L = H_2MDCPB = 5′-methyl-[1,1′,3′,1″-terphenyl]-4,4″-dicarboxylic-acid. [e] 467-MOF = $[Al_3(BTTB)_2(OH)_3](DMF)_{5.5}(H_2O)_3$, H_3BTTB = 4,4',4"-(benzene-1,3,5-triyltris(oxy))tribenzoic acid.

XIII. Comparison of proton conductivity

Table S5 Comparison of proton conductivity of **Co-2PPA** and **Co-4PPA** with some reported proton conductors.

Materials	Proton Conductivity (S/cm)	Activation Energy (eV)	Temperature (K)	RH (%)	Reference
Co-2PPA	2.96×10^{-4}	0.31	333	~97	This work
Co-4PPA	2.78×10^{-5}	0.29			
HPW@MIL-101(Cr)	7.09×10^{-6}	0.42	353	100	[11]
MIL-53(Al)	3.6×10^{-7}	0.47	353	95	[12]
MIL-53(Al)-OH, [Al(OH)(BDC-OH)] [a]	1.9×10^{-6}	0.27	353	95	
MIL-53(Fe)-$COOH_2$, [Fe(OH)(BDC-$(COOH)_2$)]	7×10^{-6}	0.21	353	95	
UiO-66(Zr)-Br	2.23×10^{-7}	0.78	303	97	[13]
β-PCMOF2(Na) [b]	5×10^{-6}	0.28	303	90	[14]
VNU-17(Zr)	6.65×10^{-6}	0.47	343	98	[15]
HIm9@VNU-17 [c]	1.53×10^{-4}	0.44	343	85	
VNU-23(Zr)	1.54×10^{-4}	–	343	90	[16]
MFM-500(Co)	4.4×10^{-5}	–	298	98	[17]
Sr-SBBA [d]	4.4×10^{-5}	0.56	298	98	[18]
CP-1(Dy)	2.96×10^{-6}	0.25	353	95	[19]
TMOF-1(Cu)	1.62×10^{-6}	0.34	363	98	[20]
{[Cd(L)(OAc)(H_2O)]OAc $\cdot9H_2O\}_n$ [e]	7.19×10^{-5}	–	383	98	[21]
$(NH_4)_2[Ag_4(mel)(NH_3)_2]$ $\cdot3H_2O$	4.3×10^{-5}	0.47	353	98	[22]
MIL-101(Cr)-SO_3H	6.32×10^{-5}	–	343	90	[23]
MOF-808(Zr)-OX	1.54×10^{-6}	0.15	303	98	[24]
HKUST-1	1.35×10^{-4}	0.33	328	95	[25]
$((CH_3)_2NH_2)_2$ $[Li_2Zr(C_2O_4)_4]$	3.9×10^{-5}	0.64	290	67	[26]
$Zn_3(IBT)_2(H_2O)_2$ [f]	1.98×10^{-5}	–	303	97	[27]

{[Fe(BTB)(H_2O)$_4$]}n (CFA-17) [g]	1.1×10^{-4}	–	296	94	[28]
$[Cu_4(L\text{-}Me_3)_3(NO_3)\cdot3H_2O]_n$ [h]	3.3×10^{-7}	0.56	298	97	[29]
$[Ce(Cbp)_3(H_2O)_3]\cdot8H_2O$ [i]	1.106×10^{-4}	0.6	368	95	[30]
$[Zn(l\text{-}LCl)(Cl)](H_2O)_2$ [j]	4.45×10^{-5}	0.34	304	98	[31]
JUC-125 [k]	1.5×10^{-4}	0.32	323	97	[32]
PMOCP 3 [l]	1.38×10^{-4}	0.14	323	97	[33]
LOF 1 [m]	9.3×10^{-5}	0.33	303	97	[34]
$\{[Pr(betc)(H_2O)_2](H_2pip)_{0.5}\}_n$ [n]	8.9×10^{-5}	0.33	313	97	[35]
$\{[Pr_2Ca(betc)_2(H_2O)_7]\cdot H_2O\}_n$	3.2×10^{-5}	0.66	305	97	[36]
OCC 2 [o]	3.72×10^{-4}	0.21	299	97	[37]
$Co(PPA)_2(BDC)(H_2O)_2\cdot(PPA)_2(H_2BDC)_2(H_2O)$ [p]	2.29×10^{-4}	0.24	325	97	[38]
SCU-17 [q]	5.87×10^{-5}	0.54	358	95	[39]
SCU-26 [r]	5.83×10^{-5}	0.66	358	95	[40]
SCU-27 [s]	9.0×10^{-4}	0.37	358	95	

[a] H_2bdc = 1,4-benzenedicarboxylic acid. [b] β-PCMOF2(Na) = 2,4, 6-trihydroxy -1,3,5-benzene-trisulfonate. [c] $HSNDC^{2-}$ = 4-sulfonaphthalene-2,6-dicarb- oxylate, Im = imidazole. [d] SBBA = 4 ,4′- sulfobisbenzoic-acid. [e] L = 2,2'-(1,4-phenylene)bis(N-(pyridin-3-yl) acetamide). [f] H_4BTC = benzene-1,2,4,5 -tetracarboxylic-acid, Im = imidazole. [g] BTB^{2-} = $C_6N_6O_2^{2-}$. [h] L^{CH_3} = 3,5-diiso-propyl-1,2,4-triazolate; S,S or R,R-L^{OH} = (S,S or R,R)-3,5-bis(1-hydroxyethyl)-1,2,4-triazolate). [i] H_2CcbpBr = 4-carboxy-1-(4-carboxybenzyl) pyridinium bromide. [j] L = 3-methyl-2-(pyridin-4-ylmethylamino) butanoic acid. [k] JUC-125 = $\{[Gd_4(R\text{-}ttpc)_2(R\text{-}Httpc)_2(HCOO)_2(H_2O)_8]\cdot4H_2O\}_n$; R-$H_3$ttpc = (3R,3′R,3″R)-1,1′,1″-(1,3,5-tria- zine-2,4,6-triyl)-tripiperidine-3-carboxylic-acid. [l] PMOCP3 = $\{Cd(D\text{-}pmpcH)(H_2O)_2Cl_2\}_n$; D-$H_3$pmpc = 1-(phosphonomethyl)piperidine-3-carboxylic-acid. [m] LOF1 = $\{[Er_3(pmpc)(C_2O_4)_3\ (H_2O)_7]\cdot2H_2O\}_n$. [n] H_4betc = 1,2,4,5-benzenetetracarboxylic acid; pip = piperazine. [o] OCC 2 = $(H_3betc)_2(H_2\text{-}Mepip)\cdot(H_2O)$; Mepip = 2-methyl-piperazine. [P] $Co(PPA)_2(BDC)(H_2O)_2\cdot(PPA)_2\ (H_2BDC)_2(H_2O)$; H_2BDC = 1,4-benzenedicarboxylic acid). [q] SCU-17 = $Hmim\cdot Fe^{II}Fe^{III}\ (HPO_3)_2\ F_2(H_2O)_2$, Hmim = 2-methylimidazolium. [r] SCU-26 = $In(HPO_4)(C_2O_4)_{0.5}$(HINT). [s] SCU-27 = $H_2INT\cdot Ga(HPO_4)(C_2O_4)\cdot H_2O$.

XIV. References

1 D. W. Feng, T. F. Liu, J. Su, M. Bosch, Z. W. Wei, W. Wan, D. Q. Yuan, Y. P. Chen, X. Wang, K. C. Wang, X. Z. Lian, Z. Y. Gu, J. H. Park, X. D. Zou and H. C. Zhou, Stable metal-organic frameworks containing single-molecule traps for enzyme encapsulation, *Nat. Commun.,* 2015, **6**, 5979.

2 D. W. Feng, K. C. Wang, J. Su, T. F. Liu, J. Y. Park, Z. W. Wei, M. Bosch, A. Yakovenko, X. D. Zou and H. C. Zhou, A highly stable zeotype mesoporous zirconium metal-organic framework with ultralarge pores, *Angew. Chem. Int. Ed.,* 2015, **54**, 149-154.

3 D. X. Xue, Y. Belmabkhout, O. Shekhah, H. Jiang, K. Adil, A. J. Cairns and M. Eddaoudi, Tunable rare earth fcu-MOF platform: Access to adsorption kinetics driven gas/vapor separations via pore size contraction, *J. Am. Chem. Soc.,* 2015, **137**, 5034-5040.

4 A. Fateeva, P. A. Chater, C. P. Ireland, A. A. Tahir, Y. Z. Khimyak, P. V. Wiper, J. R. Darwent and M. J. Rosseinsky, A water-stable porphyrin-based metal-organic framework active for visible-light photocatalysis, *Angew. Chem. Int. Ed.,* 2012, **51**, 7440-7444.

5 S. Rodriguez Hermida, M. Y. Tsang, C. Vignatti, K. C. Stylianou, V. Guillerm, J. Perez Carvajal, F. Teixidor, C. Vinas, D. Choquesillo-Lazarte, C. Verdug Escamilla, I. Peral, J. Juanhuix, A. Verdaguer, I. Imaz, D. Maspoch and J. Giner Planas, Switchable surface hydrophobicity-hydrophilicity of a metal-organic framework, *Angew. Chem. Int. Ed.,* 2016, **55**, 16049-16053.

6 X. D. Sun, S. Yao, C. Y. Yu, G. H. Li, C. M. Liu, Q. S. Huo and Y. L. Liu, An ultrastable Zr-MOF for fast capture and highly luminescence detection of $Cr_2O_7^{2-}$ simultaneously in an aqueous phase, *J. Mater. Chem. A,* 2018, **6**, 6363-6369.

7 Z. Y. Li, Z. J. Zhang, Y. X. Ye, K. C. Cai, F. F. Du, H. Zeng, J. Tao, Q. J. Lin, Y. Zheng and S. C. Xiang, Rationally tuning host-guest interactions to free hydroxide ions within intertrimerically cuprophilic metal-organic frameworks for high OH^- conductivity, *J. Mater. Chem. A,* 2017, **5**, 7816-7824.

8 Z. W. Wang, M. Chen, C. S. Liu, X. Wang, H. Zhao and M. Du, A versatile Al-III-based metal-organic framework with high physicochemical stability, *Chem. Eur. J.,* 2015, **21**, 17215-17219.

9 Y. Chen, B. Wang, X. Q. Wang, L. H. Xie, J. P. Li, Y. B. Xie and J. R. Li, A copper(II)-paddlewheel metal-organic framework with exceptional hydrolytic

stability and selective adsorption and detection ability of aniline in water, *ACS Appl. Mater. Interfaces,* 2017, **9**, 27027-27035.

10 X. J. Kong, T. He, J. Zhou, C. Zhao, T. C. Li, X. Q. Wu, K. C. Wang and J. R. Li, In situ porphyrin substitution in a Zr(IV)-MOF for stability enhancement and photocatalytic CO_2 reduction, *Small,* 2021, **17**, 2005357.

11 X. Y. Lai, Y. W. Liu, G. C. Yang, S. M. Liu, Z. Shi, Y. Lu, F. Luo and S. X. Liu, Controllable proton-conducting pathways via situating polyoxometalates in targeting pores of a metal-organic framework, *J. Mater. Chem. A,* 2017, **5**, 9611-9617.

12 A. Shigematsu, T. Yamada and H. Kitagawa, Wide control of proton conductivity in porous coordination polymers, *J. Am. Chem. Soc.,* 2011, **133**, 2034-2036.

13 F. Yang, H. L. Huang, X. Y. Wang, F. Li, Y. H. Gong, C. L. Zhong and J. R. Li, Proton conductivities in functionalized UiO-66: Tuned properties, thermogravimetry mass, and molecular simulation analyses, *Cryst. Growth Des.,* 2015, **15**, 5827-5833.

14 J. A. Hurd, R. Vaidhyanathan, V. Thangadurai, C. I. Ratcliffe, I. L. Moudrakovski and G. K. H. Shimizu, Anhydrous proton conduction at 150 °C in a crystalline metal-organic framework, *Nat. Chem.,* 2009, **1**, 705-710.

15 T. H. N. Lo, M. V. Nguyen and T. N. Tu, An anchoring strategy leads to enhanced proton conductivity in a new metal-organic framework, *Inorg. Chem. Front.,* 2017, **4**, 1509-1516.

16 M. V. Nguyen, T. H. N. Lo, L. C. Luu, H. T. T. Nguyen and T. N. Tu, Enhancing proton conductivity in a metal-organic framework at T > 80 ℃ by an anchoring strategy, *J. Mater. Chem. A,* 2018, **6**, 1816-1821.

17 S. Pili, S. P. Argent, C. G. Morris, P. Rought, V. Garcia Sakai, I. P. Silverwood, T. L. Easun, M. Li, M. R. Warren, C. A. Murray, C. C. Tang, S. Yang and M. Schroeder, Proton conduction in a phosphonate-based metal-organic framework mediated by intrinsic "free diffusion inside a sphere", *J. Am. Chem. Soc.,* 2016, **138**, 6352-6355.

18 T. Kundu, S. C. Sahoo and R. Banerjee, Alkali earth metal (Ca, Sr, Ba) based thermostable metal-organic frameworks (MOFs) for proton conduction, *Chem. Commun.,* 2012, **48**, 4998-5000.

19 S. P. Bera, A. Mondal, S. Roy, B. Dey, A. Santra and S. Konar, 3D isomorphous

lanthanide coordination polymers displaying magnetic refrigeration, slow magnetic relaxation and tunable proton conduction, *Dalton Trans.,* 2018, **47**, 15405-15415.

20 G. Y. Zhang and H. H. Fei, Missing metal-linker connectivities in a 3-D robust sulfonate-based metal-organic framework for enhanced proton conductivity, *Chem. Commun.,* 2017, **53**, 4156-4159.

21 K. Maity, T. Kundu, R. Banerjee and K. Biradha, One-dimensional water cages with repeat units of $(H_2O)(24)$ resembling pagodane trapped in a 3D coordination polymer: proton conduction and tunable luminescence emission by adsorption of anionic dyes, *CrystEngComm,* 2015, **17**, 4439-4443.

22 X. Y. Dong, X. Li, B. Li, Y. Y. Zhu, S. Q. Zang and M. S. Tang, Water sandwiched by a pair of aromatic rings in a proton-conducting metal-organic framework, *Dalton Trans.,* 2016, **45**, 18142-18146.

23 X. M. Li, L. Z. Dong, S. L. Li, G. Xu, J. Liu, F. M. Zhang, L. S. Lu and Y. Q. Lan, Synergistic conductivity effect in a proton sources-coupled metal organic framework, *ACS Energy Lett.,* 2017, **2**, 2313-2318.

24 X. Meng, H. N. Wang, L. S. Wang, Y. H. Zou and Z. Y. Zhou, Enhanced proton conductivity of a MOF-808 framework through anchoring organic acids to the zirconium clusters by post-synthetic modification, *CrystEngComm,* 2019, **21**, 3146-3150.

25 S. L. Wang, P. P. Li, S. K. Fan, Z. Fang, X. B. Wang, Z. Y. Li and X. S. Peng, A unique photoswitch: intrinsic photothermal heating induced reversible proton conductivity of a HKUST-1 membrane, *Dalton Trans.,* 2021, **50**, 2731-2735.

26 S. Tominaka, F. X. Coudert, T. D. Dao, T. Nagao and A. K. Cheetham, Insulator-to-proton-conductor transition in a dense metal-organic framework, *J. Am. Chem. Soc.,* 2015, **137**, 6428-6431.

27 X. X. Xie, Y. C. Yang, B. H. Dou, Z. F. Li and G. Li, Proton conductive carboxylate-based metal-organic frameworks, *Coord. Chem. Rev.,* 2020, **403**, 213100.

28 H. Bunzen, A. Javed, D. Klawinski, A. Lamp, M. Grzywa, A. Kalytta Mewes, M. Tiemann, H. A. K. Von Nidda, T. Wagner and D. Volkmer, Anisotropic water-mediated proton conductivity in large iron(II) metal-organic framework single crystals for proton-exchange membrane fuel cells, *ACS Appl. Nano Mater.,* 2019, **2**, 291-298.

29 B. Q. Song, D. Q. Chen, Z. G. Ji, J. H. Tang, X. L. Wang, H. Y. Zang and Z. M. Su, Control of bulk homochirality and proton conductivity in isostructural chiral metal-organic frameworks, *Chem. Commun.,* 2017, **53**, 1892-1895.

30 Z. L. Bai, Y. L. Wang, W. Liu, Y. X. Li, J. Xie, L. H. Chen, D. P. Sheng, D. W. Juan, Z. F. Chai and S. A. Wang, Significant proton conductivity enhancement through rapid water induced structural transformation from a cationic framework to a water-rich neutral chain, *Cryst. Growth Des.,* 2017, **17**, 3847-3853.

31 S. C. Sahoo, T. Kundu and R. Banerjee, Helical water chain mediated proton conductivity in homochiral metal-organic frameworks with unprecedented zeolitic unh-topology, *J. Am. Chem. Soc.,* 2011, **133**, 17950-17958.

32 X. Liang, F. Zhang, H. Zhao, W. Ye, L. Long and G. Zhu, A proton-conducting lanthanide metal-organic framework integrated with a dielectric anomaly and second-order nonlinear optical effect, *Chem. Commun.,* 2014, **50**, 6513-6516.

33 X. Liang, K. Cai, F. Zhang, J. Liu and G. Zhu, One, two, and three-dimensional metal-organic coordination polymers derived from enantiopure organic phosphorate: homochirality, water stability and proton conduction, *CrystEngComm,* 2017, **19**, 6325-6332.

34 X. Liang, K. Cai, F. Zhang, J. Liu and G. Zhu, A proton-conductive lanthanide oxalatophosphonate framework featuring unique chemical stability: stabilities of bulk phase and surface structure, *J. Mater. Chem. A,* 2017, **5**, 25350-25358.

35 X. Liang and Z. Fan, Structural characterization and proton-conductive property of a lanthanide metal-organic framework assembled from 1,2,4,5-Benzenetetracarboxylic acid and piperazine, *Chin. J. Struct. Chem.,* 2017, **36**, 977-984.

36 X. Liang, R. Li and Z. Fan, Hydrothermal synthesis, crystal structure and proton conductivity of a Pr-Ca heterometal-organic framework generated by 1,2,4,5-Benzenetetracarboxylic acid, *Chin. J. Struct. Chem.,* 2017, **36**, 993-1002.

37 X. Liang, Y. Chen, L. Wang, F. Zhang, Z. Fan, T. Cao, Y. Cao, H. Zhu, X. He, B. Deng, Y. You, Y. Dong and Y. Zhao, Effect of carbon-skeleton isomerism on the dielectric properties and proton conduction of organic cocrystal compounds assembled from 1,2,4,5-benzenetetracarboxylic acid and piperazine derivatives, *New J. Chem.,* 2019, **43**, 11099-11112.

38 X. Liang, T. Cao, L. Wang, C. Zheng, Y. Zhao, F. Zhang, C. Wen, L. Feng and C. Wan, From an organic ligand to a metal-organic coordination polymer, and to

a metal-organic coordination polymer-cocrystal composite: a continuous promotion of the proton conductivity of crystalline materials, *CrystEngComm,* 2020, **22**, 1414-1424.

39 T. Li, Y. Mao, Y. Qi, H. Zeng, G. Zou and Z. Lin, Ionothermal synthesis of crystalline metal phosphites using multifunctional protic ionic liquids, *CrystEngComm,* 2020, **22**, 6096-6100.

40 L. Huang, H. Xu, Y. Zhao, L. Huang, J. Bi, H. Zeng, G. Zou, D. Gao and Z. Lin, Isonicotinic acid-templated metal phosphate-oxalates: solvent-free synthesis, luminescence, and proton conduction, *CrystEngComm,* 2021, **23**, 6855-6858.